

See discussions, stats, and author profiles for this publication at: <https://www.researchgate.net/publication/264201656>

# Photon upconversion in core-shell nanoparticles

ARTICLE *in* CHEMICAL SOCIETY REVIEWS · JULY 2014

Impact Factor: 33.38 · DOI: 10.1039/c4cs00151f · Source: PubMed

---

CITATIONS

20

READS

68

---

## 4 AUTHORS, INCLUDING:



Dengfeng Peng  
City University of Hong Kong  
33 PUBLICATIONS 330 CITATIONS

[SEE PROFILE](#)



Feng Wang  
City University of Hong Kong  
41 PUBLICATIONS 5,540 CITATIONS

[SEE PROFILE](#)



Cite this: DOI: 10.1039/c4cs00151f

## Photon upconversion in core–shell nanoparticles

Xian Chen,<sup>a</sup> Denfeng Peng,<sup>a</sup> Qiang Ju<sup>a</sup> and Feng Wang<sup>\*ab</sup>

Photon upconversion generally results from a series of successive electronic transitions within complex energy levels of lanthanide ions that are embedded in the lattice of a crystalline solid. In conventional lanthanide-doped upconversion nanoparticles, the dopant ions homogeneously distributed in the host lattice are readily accessible to surface quenchers and lose their excitation energy, giving rise to weak and susceptible emissions. Therefore, present studies on upconversion are mainly focused on core–shell nanoparticles comprising spatially confined dopant ions. By doping upconverting lanthanide ions in the interior of a core–shell nanoparticle, the upconversion emission can be substantially enhanced, and the optical integrity of the nanoparticles can be largely preserved. Optically active shells are also frequently employed to impart multiple functionalities to upconversion nanoparticles. Intriguingly, the core–shell design introduces the possibility of constructing novel upconversion nanoparticles by exploiting the energy exchange interactions across the core–shell interface. In this *tutorial review*, we highlight recent advances in the development of upconversion core–shell nanoparticles, with particular emphasis on the emerging strategies for regulating the interplay of dopant interactions through core–shell nanostructural engineering that leads to unprecedented upconversion properties. The improved control over photon energy conversion will open up new opportunities for biological and energy applications.

Received 3rd May 2014

DOI: 10.1039/c4cs00151f

[www.rsc.org/csr](http://www.rsc.org/csr)

### Key learning points

- (1) Identify the advantage of upconversion among various spectral conversion processes.
- (2) Understand the optical transitions involved in lanthanide-doped nanoparticles.
- (3) Recognise the criteria for composing upconversion core–shell nanoparticles.
- (4) Understand the strategies for synthesizing upconversion core–shell nanoparticles.
- (5) Appreciate the effect of core–shell structural engineering on tuning upconversion.

## 1. Introduction

Near infrared (NIR) light is an important part of the electromagnetic spectrum that is invisible to human, non-destructive and abundant in nature. In comparison to ultraviolet and visible light, NIR light is also easier to generate in the form of laser radiation. Therefore, it is generally considered as an ideal light source for a variety of modern-day technologies including displays, photovoltaics, data storage, and cancer therapy.<sup>1</sup> However, most processes and techniques cannot effectively make use of NIR light due to their insufficient photon energies. The problem has fuelled a growing demand for the development of spectral converters that can be readily integrated into various applications.

NIR light can be converted into higher energy photon emissions *via* several distinct strategies. Second-harmonic generation (SHG) and two-photon absorption (TPA) are well-established methods for performing photon frequency conversion. However, there are inherent limitations associated with these two methods because only high density NIR photon flux ( $10^6\text{--}10^9 \text{ W cm}^{-2}$ ) delivered by expensive pulsed lasers can be converted due to the involvement of non-stationary quantum mechanical states. Photon upconversion (UC) through the use of lanthanide ions is a promising alternative for the spectral conversion of NIR light. In addition, UC differs from SHG and TPA in that the process is based on optical transitions between physically existing intermediary energy states (Fig. 1), thereby allowing more efficient spectral conversion without the need for intense coherent NIR light sources. This method also has the benefit of large anti-Stokes shifts, sharp emission bandwidths, long excited-state lifetimes, and tunable emission by single wavelength excitation.

<sup>a</sup> Department of Physics and Materials Science, City University of Hong Kong, 83 Tat Chee Avenue, Hong Kong SAR, China. E-mail: fwang24@cityu.edu.hk; Fax: +852 3442 0538; Tel: +852 3442 4898

<sup>b</sup> City University of Hong Kong Shenzhen Research Institute, Shenzhen 518057, China

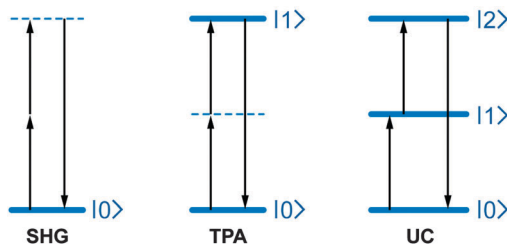


**Fig. 1** Simplified energy level diagrams depicting typical anti-Stokes processes. In a SHG (also called frequency doubling) process, the frequency of irradiated light is doubled without any absorption transitions taking place. TPA involves the simultaneous absorption of two photons. UC processes feature sequential absorption of the excitation energy through the use of long-lived intermediary energy states.

Photon UC was discovered in the 1960s. However, UC nanoparticles did not appear until the 2000s, largely due to the

increased difficulties in performing UC in nanoparticles characterized by large surface areas. Lanthanide ions generally feature long excited-state lifetimes in the micro- to millisecond range that increases the chance of deactivation through nonradiative channels typically associated with surface defects, impurities and containments. UC emissions are particularly vulnerable to the nonradiative relaxations because the depletion of either the emitting states or the intermediate reservoir states inhibits a UC process. The prevalence of UC nanoparticle research in recent years is largely promoted by advances in synthetic chemistry that have allowed facile access to lanthanide-doped nanoparticles with well-defined structure, size, and surface properties.

Conventional UC nanoparticles can be generally regarded as the nanoscale version of their bulk counterparts because UC properties are essentially independent of particle size. Intra-4f transitions of lanthanide ions are ionic properties and unaffected



**Xian Chen**

research focuses on the development of novel lanthanide-doped luminescent nanomaterials.

*Xian Chen was born in Zhejiang, China, in 1987. He received his BE degree (2009) in Materials Science and Engineering from Huazhong University of Science and Technology and MS degree (2012) in Materials Science and Engineering from Zhejiang University. He is currently pursuing a PhD degree under the supervision of Prof. Feng Wang in the Department of Physics and Materials Science at City University of Hong Kong. His*



**Dengfeng Peng**

rare earth nanostructured optoelectronic and advanced energy devices.

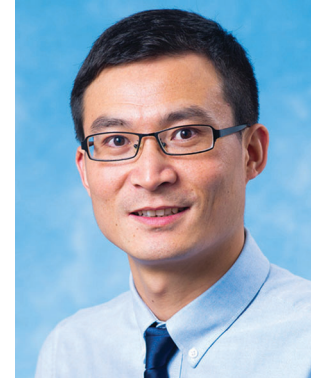
*Dengfeng Peng was born in Hubei, China. He received his BS degree (2006) in Physics from Xinjiang University and PhD degree (2013) in Materials Science and Engineering from Tongji University. He spent one year as a joint PhD student at National Institute of Advanced Industrial Science and Technology in Japan. He joined the group of Prof. Feng Wang at City University of Hong Kong in 2013. His research interests include design and synthesis of materials for applications in*



**Qiang Ju**

*University Bochum (2011–2012) and with Prof. Ulrich J. Krull at University of Toronto (2012–2013). He joined the group of Prof. Feng Wang at City University of Hong Kong in 2013. His research focuses on the bioapplication of lanthanide-doped nanoparticles.*

*Qiang Ju was born in Shandong, China, in 1983. He received his BS degree (2005) in Chemistry from Qufu Normal University. He earned his PhD degree (2010) in Materials Physics and Chemistry from Fujian Institute of Research on the Structure of Matter (FJIRSM), Chinese Academy of Sciences (CAS), under the supervision of Prof. Xueyuan Chen. He then carried out postdoctoral research work with Prof. Anja-Verena Mudring at Ruhr*



**Feng Wang**

*Institute of Materials Research and Engineering in Singapore. He joined the faculty of City University of Hong Kong in 2012. His research interests include the design, synthesis, mechanistic investigation, and application of luminescent nanomaterials.*

*Feng Wang was born in Shaanxi, China. He received his BE (2001) and PhD (2006) degrees in Materials Science and Engineering from Zhejiang University. His PhD thesis was focused on the synthesis and characterization of lanthanide-doped fluoride nanomaterials under the supervision of Prof. Mingquan Wang and Prof. Xianping Fan. He then carried out postdoctoral research work with Prof. Xiaogang Liu at the National University of Singapore and the*

by quantum size effects that dictate electronic transitions in the crystal lattice. The changes in UC emission profiles frequently observed in nanoparticle hosts are usually correlated with the surface states, which are characterized by imperfect crystal lattices and high densities of impurities. Despite an ineffective tuning of optical emissions, the small particle size can lead to a number of desirable characteristics, including good colloidal stability and high processability, which are critical prerequisites<sup>2,3</sup> for emerging applications in the fields of biology and energy.<sup>2,3</sup>

The use of a core-shell structured host has provided exciting new opportunities for UC research. The idea of core-shell design was inspired by a study on semiconductor quantum dots (QDs) that take advantage of a protection shell to suppress nonradiative recombination occurring at the particle surface.<sup>4</sup> UC core-shell nanoparticles were originally developed to boost UC efficiencies by growing an undoped shell layer around the core particle that minimizes the influence of surface states on the optical transitions. In the subsequent studies, multishelled nanostructures comprising optically active shells are increasingly employed for integrating functionality and for exploiting the core-shell synergy. Importantly, core-shell nanostructural engineering introduces a new variable (core-shell combination) into materials design, thereby offering substantial flexibility for constructing UC nanoparticles.

This tutorial review primarily focuses on recent progress in the deliberate control over UC by taking advantage of core-shell nanostructures. We attempt to highlight the possibility of expanding the scope of UC by manipulating the interplay of lanthanide interactions at the nanoscale. In Section 2, we present an overview of important optical processes in lanthanide ions that define the rules for constructing efficient UC nanoparticles. In Section 3, we provide general approaches for the fabrication of high quality core-shell nanoparticles with well-defined size, shell thickness, and composition. Exquisite control over nanoparticle formation is essential for the integration and coordination of dissimilar optical entities contributing to an efficient UC process. In Section 4, we discuss the effect of core-shell structural engineering on several aspects of UC, which is typically unexpected in conventional bulk materials.

## 2. Designing upconversion nanoparticles

Spectral conversion in UC nanoparticles is essentially accomplished by electronic transitions within the 4f orbitals of special lanthanide ions that are placed in an appropriate crystalline environment. Shielded by 5s and 5p subshells, f-f transitions typically give rise to well-defined optical spectra that are hardly affected by the chemical composition or physical dimension of the host materials. For rational photon UC, one has to cascade the electronic transitions of dissimilar lanthanide ions together with other optical entities to tune the absorption and emission properties. Therefore, the main task of UC nanoparticle design is to recruit appropriate lanthanide ions into a single nanoparticle and to regulate their interplay with the surroundings.

### 2.1 Lanthanide energy transfer

A distinct characteristic of UC nanoparticles is the presence of a large number of dopant ions in individual particles that extensively exchange energies with each other. Energy transfer may strongly modify the optical transitions of the dopant ions and is a critical consideration in designing UC nanoparticles.

Energy transfer generally occurs by two basic mechanisms (Fig. 2). The first mechanism is radiative reabsorption in which the donor emits a photon that is subsequently absorbed by the acceptor. Radiative reabsorption can be considered a combination of two independent luminescence processes whose excited state dynamics are unaffected by the energy transfer. Radiative energy transfer that can operate over a very long distance is commonly observed for acceptors, such as QDs and organic dyes featuring broad and intense absorptions.<sup>5</sup> However, this process is not effective for the majority of lanthanide acceptors due to the narrow absorption bands and substantially low molar extinction coefficients ( $\sim 1 \text{ M}^{-1} \text{ cm}^{-1}$ ).<sup>6</sup>

Energy transfer between lanthanide ions is typically dominated by the second mechanism in which an acceptor extracts energy from an excited donor through radiationless exchange (Dexter energy transfer) or multipolar (Förster energy transfer) interactions (Fig. 3a). In contrast with radiative reabsorption, nonradiative energy transfer adds an extra deactivation channel to the energy donor and can significantly accelerate its decay. A decrease in the donor lifetime is an explicit indication of nonradiative energy transfer, which is frequently used to quantify the energy transfer efficiency.

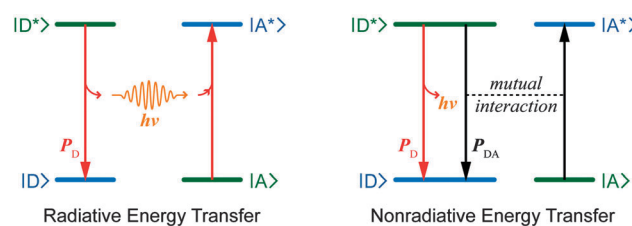


Fig. 2 Principle energy transfer processes between a donor (D) and an acceptor (A). The initial and final states are indicated by green and blue lines, respectively.  $P_D$  and  $P_{DA}$  are the radiative and nonradiative decay rates of the donor, respectively. Nonradiative relaxation by emission of phonons is not shown for simplicity.

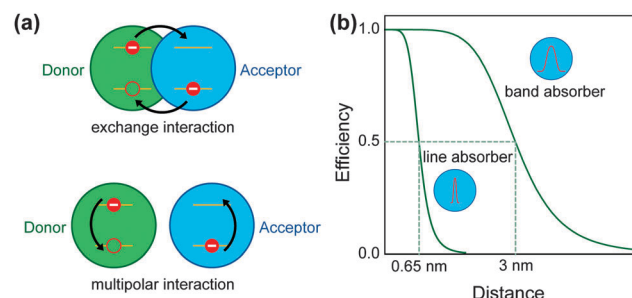


Fig. 3 (a) Schematic illustration of energy transfer through exchange and multipolar interactions, respectively. (b) The effect of transition strength in acceptor on the critical distance of a multipolar transfer. The energy transfer efficiency is defined as  $P_{DA}/(P_{DA} + P_D)$ .

The probability of a nonradiative energy transfer is strongly dependent on the donor–acceptor distance. For an exchange interaction that needs wave function overlap, the probability decreases exponentially and typically vanishes for separations beyond 0.5 nm. Energy transfers for larger separations are usually dominated by multipolar interactions, and the distance dependence is approximated by  $R^{-6}$ . A critical distance ( $R_c$ ) at which  $P_{DA}$  equals  $P_D$  is frequently used to estimate the operation range of a multipolar transfer. Depending on the strength of the optical transitions involved,  $R_c$  varies over a large distance range (Fig. 3b).<sup>7</sup>

For a nonradiative energy transfer to proceed, the donor and the acceptor should also have reasonable spectral overlap (resonance condition). Particularly, lanthanide ions of the same sort usually give rise to fully resonant energy transfers that are highly reversible. If a set of identical ions are arrayed with a short interionic distance, the excitation energy may randomly hop among these ions. This process is recognized as energy migration and can deliver the excitation energy to a site over a 10 nm distance from the original donor.<sup>7</sup>

Lanthanide ions featuring a multiplicity of excited states can result in a diversity of energy transfer processes that eventually lead to distinct consequences. In most cases, the donor will give all the energy to the acceptor for sensitizing optical emissions of the latter (Fig. 4a). Alternatively, a donor ion often shows a partial energy transfer known as cross-relaxation (Fig. 4b). The effect has been harnessed to tune the donor emission or to perform down-conversion quantum cutting.<sup>8</sup> Furthermore, energy transfer is also possible to an acceptor that is already in an excited state (Fig. 4c), which was first recognized by Auzel and represents a key step in the discovery of UC.<sup>9</sup> This type of energy transfer is also observed in some organic compounds, resulting in a particular UC process called triplet-triplet annihilation (TTA).<sup>10</sup>

Taking advantage of the energy transfer for designing UC nanoparticles is limited by several factors. If energy transfer occurs by a population in the excited state featuring a narrow energy gap to the next lower-lying state, nonradiative multiphonon relaxations usually abide by the energy gap law. One representative example is the self-quenching of  $\text{Sm}^{3+}$  ions due to the cross-relaxation between  $^4\text{G}_{5/2} \rightarrow ^6\text{F}_{9/2}$  and  $^6\text{H}_{5/2} \rightarrow ^6\text{F}_{9/2}$ .<sup>7</sup> The effect also accounts for the consumption of  $\text{Yb}^{3+}$  energy in typical UC processes by lanthanide ions such as  $\text{Tb}^{3+}$ ,  $\text{Eu}^{3+}$ ,  $\text{Sm}^{3+}$ ,

$\text{Dy}^{3+}$ , and  $\text{Nd}^{3+}$  that exhibit closely spaced energy levels in the low energy region (0–10 000 cm<sup>-1</sup>). Nonradiative relaxation also frequently results from electronic transitions between ion pairs, such as  $\text{Ce}^{3+}/\text{Eu}^{3+}$ ,  $\text{Ce}^{3+}/\text{Yb}^{3+}$ , and  $\text{Tb}^{3+}/\text{V}^{5+}$  that display opposite reduction–oxidation properties, although the conditions for energy transfer are also met. The quenching effects impose stringent control over the dopant composition and concentration for maximizing optical emissions.

## 2.2 Role of host lattice in energy transfer

Host materials play important roles in the luminescence processes of lanthanide ions. Apart from promoting the f-f electronic transitions within individual lanthanide ions through perturbing the 4f wave functions by crystal field, the host lattice strongly affects the energy exchange interactions between dopant ions in several independent ways.

The crystal field that affects the spectral position of an optical transition may satisfy resonance conditions that lead to efficient energy transfers. The crystal field is essential for lanthanide energy transfer as lanthanide ions typically feature very narrow emission and absorption bands that are unfavourable to the spectral overlap. The impact of the crystal field on energy transfer is most prominent in the host lattice comprising multiple active sites because the probability of an efficient resonant or near resonant process is significantly increased. The effect has been used to account for the efficient energy transfer upconversion observed in hexagonal phase  $\text{NaYF}_4$  hosts.<sup>1</sup>

Lattice vibrations (phonons) can also facilitate energy transfers that are out of resonance by making up the energy mismatch.<sup>3</sup> Phonon participation is essential for energy transfer between dissimilar lanthanide ions because their transition lines coincide very accidentally. Phonon-assisted energy transfer could be highly efficient depending on the amount of energy mismatch and phonon energy in the host lattice. One representative example is  $\text{NaGdF}_4:\text{Ce/Tb}$  featuring a high quantum yield close to unity that makes use of phonon-assisted energy transfer from  $\text{Gd}^{3+}$  to  $\text{Tb}^{3+}$  with an energy mismatch of around 800 cm<sup>-1</sup>.<sup>7</sup> The importance of phonons in lanthanide interactions may also partly account for the inefficient UC in host materials, such as bromides featuring extremely low phonon energies, despite the largely minimized nonradiative relaxation caused by multiphonon emission.<sup>11</sup>

The interionic distance of dopant ions that determines the strength of energy transfer can be precisely controlled by manipulating the dopant concentration and crystal structure of the host lattice. Lanthanide dopant ions will be tightly held at crystallographic sites of well-defined positions when doped in a crystalline host. High dopant concentration typically guarantees the presence of dopant ions at neighbouring lattice positions and enhances energy transfer efficiencies. By controlling the distance of lattice positions occupied by lanthanide dopant ions via the selection of crystal lattice, energy transfer within the particle can be further tuned. The intraparticle energy transfer can even be localized at sub-lattice levels in host materials featuring unevenly spaced lattice positions.<sup>12</sup>

The use of core–shell nanostructure allows flexible control over dopant distributions in a manner that is essentially

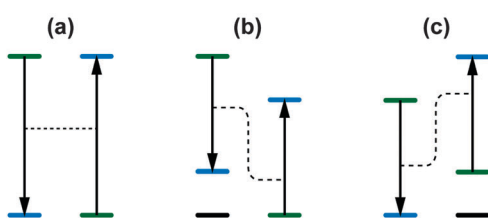


Fig. 4 Typical energy transfer processes for lanthanide ions. (a) The donor gives all the energy to the acceptor. (b) The donor only gives part of the energy to the acceptor. (c) Energy transfer to an excited acceptor. The green and blue lines represent the initial and final states, respectively. The black line indicates the ground states that are not involved in the energy transfer processes.

independent of the host lattice, thereby opening up new opportunities for regulating dopant interactions. For example, incompatible dopant ions can be spatially confined in separate layers of a core–shell nanoparticle to eliminate short-range cross-relaxations that quench luminescence. A long-range energy migration process could be further harnessed to bridge desired energy transfers across the core–shell interface.

### 2.3 Composing upconversion core–shell nanoparticles

Advances in materials chemistry have produced a wide diversity of core–shell nanoparticles composed of noble metals, semiconductors, ferromagnets, polymers, and a combination of dissimilar materials. However, most of these core–shell nanoparticles are not suitable for UC either because they are chemically incompatible with lanthanide dopants or because the radiative transitions of lanthanide ions are largely suppressed in the matrices.

UC core–shell nanoparticles usually employ a rare earth/alkaline earth fluoride core to host the UC process. These fluorides display low energy phonons ( $<500\text{ cm}^{-1}$ ) and can accommodate a high concentration of lanthanide dopant ions, which are essential for facilitating UC processes. In addition, they display high chemical and thermal stability, thereby allowing for the rational construction of various core–shell architectures (Fig. 5) without losing the structural integrity.

The shell layers that are mainly designed to alter or to decorate the UC processes occurring at the core levels can be designed with substantial flexibility. In addition to a dense surface coverage with crystalline layers matching the core nanoparticle lattice (epitaxial shell), optical components, including fluorescent dyes, QDs, and noble metals can also be attached to the surface of the core nanoparticle by forming an assembly layer or through the use of a polymeric layer (nonepitaxial shell). Epitaxial coatings offer high photochemical stability and facile formation of multi-shelled structures. Due to largely eliminated nonradiative decay channels, epitaxial core–shell structures are mainly designed to maximize the radiative spectral conversion processes. Nonepitaxially coating is virtually not constrained by the shell

composition and crystallinity, allowing the maximal modulation of optical properties. However, as nonradiative relaxations are usually dominated at the nonepitaxial core–shell interface, the combined use of epitaxial and nonepitaxial shell coatings may be necessary to realize the desired properties.

## 3. Synthesis of core–shell nanoparticles

The UC core–shell nanoparticles are generally synthesized through a layer-by-layer coating process that involves the deposition of shell layers on the surface of preformed core nanoparticles. The synthesis of high quality core nanoparticles that primarily determine the size and morphology of the final particles represents a critical prerequisite for the formation of high quality core–shell nanoparticles.

### 3.1 Synthesis of fluorides core nanoparticles

A wide variety of chemical techniques have been demonstrated to synthesize lanthanide-doped nanoparticles. However, the fabrication of fluoride nanoparticles with narrow size distributions and high colloidal stability usually requires special methods that involve thermal decomposition in coordinating solvents and controlled co-precipitation through the liquid–solid-solution (LSS) or the oleate route.

**3.1.1 Thermal decomposition.** The thermal decomposition synthesis is based on thermolysis of metal trifluoroacetates (TFA) at elevated temperatures. The reaction was first harnessed for the synthesis of high quality binary  $\text{LaF}_3$  nanoparticles in 2005 by Yan *et al.*<sup>13</sup> In their study, lanthanum trifluoroacetate was first prepared by incubating lanthanum oxide with trifluoroacetic acid at 80 °C overnight. The mixture was then purified and heated in a binary solvent mixture of oleic acid (OA) and 1-octadecene (ODE) to obtain nanoparticles. The non-coordinating ODE was used as a primary solvent due to its high boiling point (315 °C). OA was chosen not only as a solvent but also as a passivating ligand to control the nanoparticle growth and to prevent the nanoparticles from aggregation.

The thermolysis reaction can be readily extended to ternary fluoride nanoparticles by including alkali trifluoroacetates in the precursor. Notably, Yan *et al.*<sup>14</sup> employed a ternary solvent mixture of OA/OM/ODE to synthesize a group of rare earth fluoride sodium nanoparticles. They showed that the reaction can be manipulated through controlling the ratio of OA to OM and the reaction temperature. Based on these observations, the method has been developed as a common route for the synthesis of high quality UC nanoparticles with exquisite control over particle size and morphology (Fig. 6a–c).<sup>15–17</sup>

The thermal decomposition method is typically carried out at relatively high temperatures (~300 °C), allowing the synthesis of highly crystalline nanoparticles within one hour. However, the quick chemical reaction imposes strict control over the temperature to spatially separate the nucleation and growth processes, which are essential for the formation of monodisperse nanoparticles. Likewise, the decomposition of metal trifluoroacetates

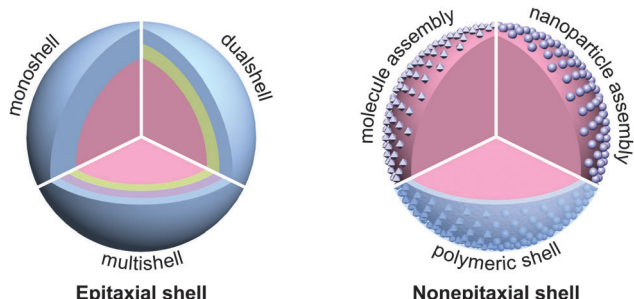
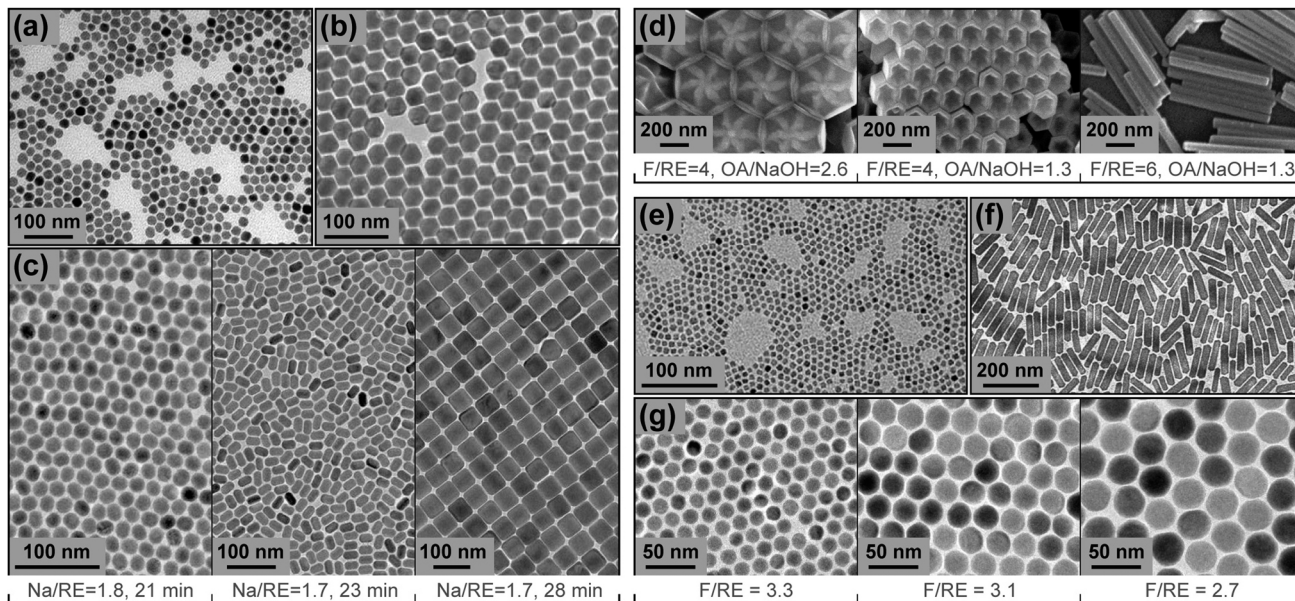


Fig. 5 Schematic illustration of the typical architectures of UC core–shell nanoparticles. For nanoparticles comprising an epitaxial shell, the entire nanoparticle displays a highly uniform structure and multilayered shells can be easily formed. In contrast, the structural uniformity discontinues at the core–shell interface for nonepitaxial core–shell nanoparticles. An epitaxial core–shell nanoparticle also frequently serves as the core nanoparticle for the nonepitaxial shell coating.



**Fig. 6** Electron micrographs of typical fluoride UC nanoparticles. (a–c)  $\alpha$ -NaYbF<sub>4</sub>:Tm,  $\alpha$ -NaGdF<sub>4</sub>:Yb/Er, and  $\beta$ -NaYF<sub>4</sub>:Yb/Er nanoparticles synthesized by thermal decomposition, respectively. (d)  $\beta$ -NaYF<sub>4</sub>:Yb/Er nanoparticles prepared through the LSS strategy. (e–g) CaF<sub>2</sub>:Yb/Er, KYb<sub>2</sub>F<sub>7</sub>:Er, and  $\beta$ -NaGdF<sub>4</sub>:Yb/Tm nanoparticles synthesized by the oleate route, respectively. Reproduced from ref. 12, 15–17, 19, 23 and 26, respectively.

produces various fluorinated and oxyfluorinated carbon species that have become a matter of environmental concern.

**3.1.2 LSS strategy.** The LSS method is based on a phase transfer and separation occurring at the interfaces of the ethanol-linoleic acid mixture (liquid), metal linoleate (solid), and water-ethanol solution containing metal ions (solution). The approach was first proposed in 2005 by Li *et al.*<sup>18</sup> as a general strategy for the synthesis of various nanoparticles, including noble metals, semiconductors, conducting polymers, and rare earth compounds.

The synthesis of lanthanide-doped fluorides nanoparticles through LSS strategy typically involves the dispersion of metal salts (chlorides or nitrates) in a ternary solvent of OA-ethanol-water charged with NaOH. The subsequent addition of NaF or NH<sub>4</sub>F and heat treatment at elevated temperatures (100–200 °C) in specialized autoclaves promotes the precipitation and growth of fluoride nanoparticles. As the synthetic conditions, such as precursor concentration, solvent composition, as well as the reaction temperature and time can be independently tuned, the method has given access to lanthanide-doped fluoride nanoparticles with controllable phase, shape, and size. Zhang and Zhao *et al.*<sup>19</sup> have demonstrated the fine tuning morphology of hexagonal phase NaYF<sub>4</sub> from nanoplates to nanoprisms and nanorods through a combined control of NaOH and fluoride concentrations (Fig. 6d).

One prominent advantage of the LSS method is the use of water as the solvent, which is compatible with a wide variety of inorganic precursors, thereby allowing cost-effective and environmentally benign synthesis of nanoparticles. However, the use of a tightly sealed reaction vessel restrains access to the reaction mixture during the synthesis. In addition, most autoclaves are incompatible with high reaction temperatures (>200 °C) and heating for a prolonged time period (up to several days) is often

required to complete the synthesis. Due to possible Ostwald ripening and recrystallization processes during the crystal growth, relatively large nanoparticles are usually produced.

**3.1.3 Oleate route.** The oleate route was devised in 2008 to synthesize sodium yttrium fluoride nanoparticles by the groups of Yan and Zhang.<sup>20,21</sup> The synthesis generally begins with an OA-ODE solution comprising of metal oleate precursors, which can be prepared by heating inorganic metal salts in oleic acid at elevated temperatures (~150 °C). The subsequent addition of fluorides will trigger a co-precipitation reaction that leads to the formation of nanoparticles. In the studies by Yan, NaF in the solid form was used to induce the reaction, which has met limited success due to poor control over the reaction at the solid-liquid interface and to the corrosion of glass flasks by NaF. The experimental design by Zhang features a combined use of NaOH and NH<sub>4</sub>F in a methanol dispersion as the precipitator, which offers fine control over the reaction rate in parallel with minimized damage to the reaction flask. The strategy has turned out to be most successful and been widely used by the community.

The oleate route has been adapted to diverse fluoride nanoparticles. For example, van Veggel *et al.*<sup>22</sup> prepared ultra-small (2.5–8.0 nm) NaGdF<sub>4</sub> nanoparticles by controlling several experimental variables, such as the OA concentration as well as the reaction time. By slightly modifying the precursor composition, various fluoride nanoparticles, including KYb<sub>2</sub>F<sub>7</sub> and CaF<sub>2</sub> have also been produced with high crystallinity and narrow size distributions (Fig. 6e and f).<sup>12,23</sup> Wang and Liu *et al.*<sup>24–26</sup> have discovered that the effects of lanthanide doping and precipitator concentration can be harnessed to control nanoparticle formation (Fig. 6g), providing a convenient means for synthesizing high quality nanoparticles with minimum attention to solvent composition and reaction temperature.

The oleate route combines the advantages of thermal decomposition and LSS for the rapid formation of high quality fluoride nanoparticles using inexpensive raw materials. Furthermore, the nucleation and crystal growth in this reaction can be separated by carrying out the two stages at widely different temperatures, thereby minimizing the influence of temperature fluctuation on the nanoparticle quality.<sup>26</sup> However, the synthesis uses both organic and inorganic chemicals, imposing tight control over the composition of the reaction media. Consequently, the types of nanoparticles that can be accessed by this method are relatively limited. For example, the synthesis of  $\alpha$ -NaYF<sub>4</sub> and binary rare earth fluoride nanoparticles by this method does not yield good results.

### 3.2 Epitaxial shell coating

Epitaxial shells can be grown by a similar chemical procedure for core nanoparticle synthesis, except that the crystal growth mainly occurs at the surface of preformed core nanoparticles other than in the liquid phase. The epitaxial deposition of shell layers can be achieved either by injecting shell precursors into a proceeding reaction (hot-injection strategy, Fig. 7a) or by charging pre-synthesized core nanoparticles into a fresh reaction before heating (heat-up strategy, Fig. 7b). It is worth noting that shell growth is dominantly conducted in organic solvents because phase separation associated with homogeneous nucleation of shell precursors is kinetically favoured in aqueous environment.

**3.2.1 Hot-injection strategy.** The hot-injection strategy originally developed to make core–shell QDs was first adapted to synthesize NaYF<sub>4</sub>:Yb/Er@NaYF<sub>4</sub> core–shell nanoparticles in 2007 by Yi and Chow.<sup>27</sup> In their thermal decomposition synthesis, NaTFA, YTFA, YbTFA, and ErTFA were first heated in OM at 340 °C for 30 min to grow the NaYF<sub>4</sub>:Yb/Er core nanoparticles. Subsequently, an OM solution comprising of NaTFA and YTFA was injected into the reaction for the epitaxial deposition of the undoped NaYF<sub>4</sub> shell layer. In follow-up studies, several core–shell nanostructures were synthesized, including NaYbF<sub>4</sub>@CaF<sub>2</sub>, NaGdF<sub>4</sub>@NaGdF<sub>4</sub>, and LiLuF<sub>4</sub>@LiLuF<sub>4</sub>.<sup>15,28,29</sup>

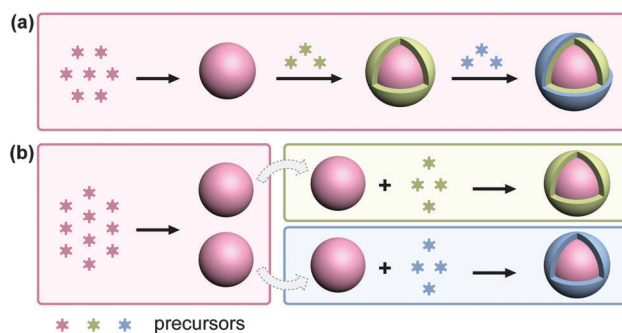


Fig. 7 Common strategies for fabricating epitaxial UC core–shell nanoparticles. (a) Rapid synthesis of multishelled nanoparticles through serial hot-injections of diverse shell precursors. (b) Facile tuning of the shell composition through a parallel heat-up of pre-synthesized core nanoparticles with varying shell precursors.

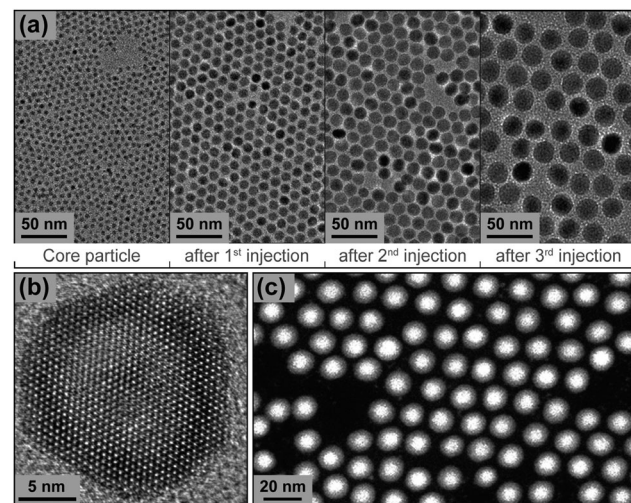


Fig. 8 (a) TEM images of NaGdF<sub>4</sub>:Yb/Er core nanoparticles and the corresponding NaGdF<sub>4</sub>:Yb/Er@NaYF<sub>4</sub> core–shell nanoparticles obtained by the successive injection of shell precursors. (b) HRTEM and image of a core–shell nanoparticle, indicating its single-crystalline nature. (c) Typical HAADF-STEM image of the core–shell nanoparticles showing high uniformity of the shell layers. Reproduced from ref. 30.

As a distinct advantage, the hot-injection strategy allows the one-pot synthesis of multishelled nanostructures through the successive injection of a sequence of shell precursors (Fig. 7a). The shell thickness can also be precisely controlled by manipulating the injection dosage. In one remarkable development, Zhang and Zhao *et al.*<sup>30</sup> described a successive layer-by-layer coating strategy for controlling the shell composition and thickness at a single atomic layer level. The method is based on the continuous injection of shell precursors at very low dosages, which tends to form uniform coating layers through a successive ion layer adsorption reaction (Fig. 8).

For a hot-injection process to proceed, the shell precursor solution must be highly compatible with the host reaction, which is typically satisfied by the thermal decomposition synthesis featuring plain precursor recipes. The constraint was overcome by van Veggel *et al.*<sup>31</sup> who proposed injecting small sacrificial nanoparticles as shell precursors. Driven by Ostwald ripening, the small nanoparticles can be quickly dissolved and deposited on the core nanoparticles. The effect enables the facile synthesis of multishelled nanoparticles through the standard oleate route (Fig. 9).

**3.2.2 Heat-up strategy.** In a typical heat-up procedure, the core and shell layers are successively grown by a sequence of independent syntheses. The idea of separating the core and shell growth processes was first conceived in 2007 by Yan *et al.*<sup>32</sup> and refined in 2008 by Qian and Zhang.<sup>33</sup> In both studies, the core nanoparticle was first synthesized and extracted from the reaction media. The as-synthesized core nanoparticles were then transferred to a fresh reaction pot to mediate the growth of the shell layer following an identical protocol for the core synthesis.

Shell thickness control in heat-up synthesis can be readily achieved by adjusting the mass ratio of the shell precursor to

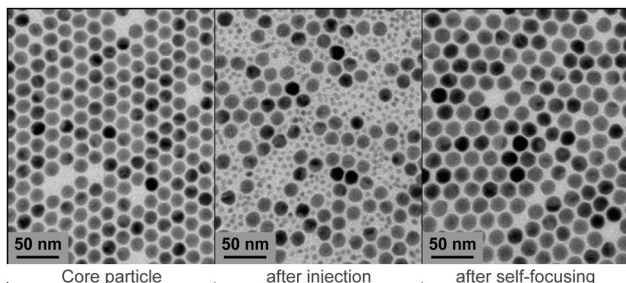


Fig. 9 TEM images of  $\text{NaYF}_4\text{:Yb}/\text{Er}$  core nanoparticles and the corresponding  $\text{NaYF}_4\text{:Yb}/\text{Er}@\text{NaYF}_4$  core–shell nanoparticles obtained by injection of small sacrificial nanoparticles. Reproduced from ref. 31.

core in the nanoparticles.<sup>6,26</sup> A precise control over the shell thickness was demonstrated by Zhang and Zhao *et al.*<sup>34</sup> who heated  $\text{NaYF}_4\text{:Yb}/\text{Er}$  nanoparticles in OA–ODE solution charged with varying amount precursors for  $\text{NaGdF}_4$  shell. By quantifying the shell precursor concentrations based on the spherical concentric shell model, they synthesized a series of  $\text{NaYF}_4\text{:Yb}/\text{Er}@\text{NaGdF}_4$  core–shell nanoparticles with a shell thickness corresponding between one and ten Gd atomic layers.

Despite being potentially laborious, the heat-up approach is equally useful for producing multishelled nanostructures by repeating the precise synthetic protocol comprising a reduced number of steps. Importantly, the solvent composition can be deliberately adjusted in the coating process, which is important for modifying epitaxial growth kinetics toward tunable shell structures.<sup>26,35</sup>

One prominent advantage of the heat-up strategy is that the pre-synthesized core nanoparticles can be used as a standard starting material to serve in a batch of succeeding coating processes (Fig. 7b). Furthermore, the strategy also allows for arbitrary combinations of dissimilar synthetic approaches for flexible core–shell fabrication. For example, the core nanoparticles can be synthesized in water by LSS method, while the shell coating can be carried out in OA–ODE through the oleate route.<sup>6</sup>

### 3.3 Nonepitaxial shell coating

Nonepitaxial shells are often deposited on pre-synthesized core nanoparticles. The shell layers can be immobilized on the surface of nanoparticles either by means of chemical bonding or through surface polymerization.

Organic molecules displaying desired optical properties have been used as shell layers of UC nanoparticles. Fluorescent molecules containing anchoring groups, such as carboxyl and phosphate can be directly coordinated to metal ions at the nanoparticle surface forming a stable assembly layer.<sup>36</sup> For molecules lacking such functional groups, a chemical modification process is often needed prior to surface coating. For example, Hummelen *et al.*<sup>37</sup> showed that carboxylic group can be grafted to a commercially available cyanine dye through the nucleophilic substitution of the central chlorine atom. The carboxylated derivative was demonstrated to replace the native OM ligand on the  $\text{NaYF}_4\text{:Yb}/\text{Er}$  nanoparticles upon incubation in  $\text{CHCl}_3$ , leading to tight surface coverage with fluorescent dyes.

Various optical nanoparticles, including noble metals and QDs are also frequently assembled on the surface of UC nanoparticles. Functional molecules are usually used to join different nanoparticles. For example, Huang and Duan *et al.*<sup>38</sup> demonstrated the construction of  $\text{NaYF}_4\text{:Yb}/\text{Tm}@\text{Au}$  heterostructures using polyelectrolytes. In their study,  $\text{NaYF}_4\text{:Yb}/\text{Tm}$  and gold nanoparticles were separately synthesized and functionalized with oppositely-charged polyions. The attachment of gold nanoparticles onto the UC nanoparticles with tunable surface coverage was achieved by mixing the nanoparticles in an aqueous solution at precisely defined ratios. A thick gold shell was also achieved by introducing additional gold precursors into the reaction mixture (Fig. 10a). In another report, Rosei and Perepichka *et al.*<sup>39</sup> described the seeded growth of CdSe on OA-capped  $\text{NaYF}_4\text{:Yb}/\text{Er}$  nanoparticles in organic solvents comprising OM. The as-synthesized nanocomposites consisted of a  $\text{NaYF}_4\text{:Yb}/\text{Er}$  core decorated with CdSe dots (Fig. 10b). The electrostatic attraction between OA and OM ligands on the surface of different nanoparticles was considered to be the driving force for the organization of binary assemblies.

Polymeric shells typically composed of silica have been employed as a versatile support platform for the installation of fluorescent dyes and optical nanoparticles. Silica shell is generally prepared using modified Stöber methods that involve the controlled hydrolysis and condensation of siloxane monomers.

The silica coating of hydrophobic UC nanoparticles usually requires the assistance of microemulsions, which create numerous nanoscale droplets in an organic solution that serve as reactors to accommodate the aqueous shell precursors. In a representative example, Li and Zhang *et al.*<sup>21</sup> demonstrated the synthesis of  $\text{NaYF}_4\text{:Yb}/\text{Er}@\text{SiO}_2$  core–shell nanoparticles comprising a highly uniform silica layer in a water–cyclohexane solution emulsified by polyoxyethylene(5)nonylphenylether (CO-520). They also showed that organic dye molecules and QDs can be included in the monomer solution and eventually encapsulated into the silica shell (Fig. 10c). In a follow-up study, Li and Xiong *et al.*<sup>40</sup> further described the functionalization of the silica shell with amino groups to immobilize gold nanoparticles on the surface (Fig. 10d).

Alternatively, a silica coating can be conducted in an aqueous solution given that the UC nanoparticles are surface modified to provide hydrophilic wetting properties. The method eliminates the precise control of surfactant content essential for creating stable micelles, thereby allowing a rational design of the solvent composition to fine tune the thickness and porosity of the silica shells (Fig. 10e and f).<sup>41,42</sup> The mesoporous silica shells should be more favourable to accommodate guest optical components. Notably, normal silica shells can also be readily coated without the need for any surfactants, thereby bypassing the tedious purification steps and largely avoiding the formation of necking between the silica beads.<sup>43</sup> Typically, dense silica shell can serve as a general substrate for attaching various optical molecules or nanoparticles through well-established silica surface chemistry. When compared with direct surface coupling, the incorporation of a silica interlayer can lead to improved chemical stability along with tunable separation between the core and surface tethered components.

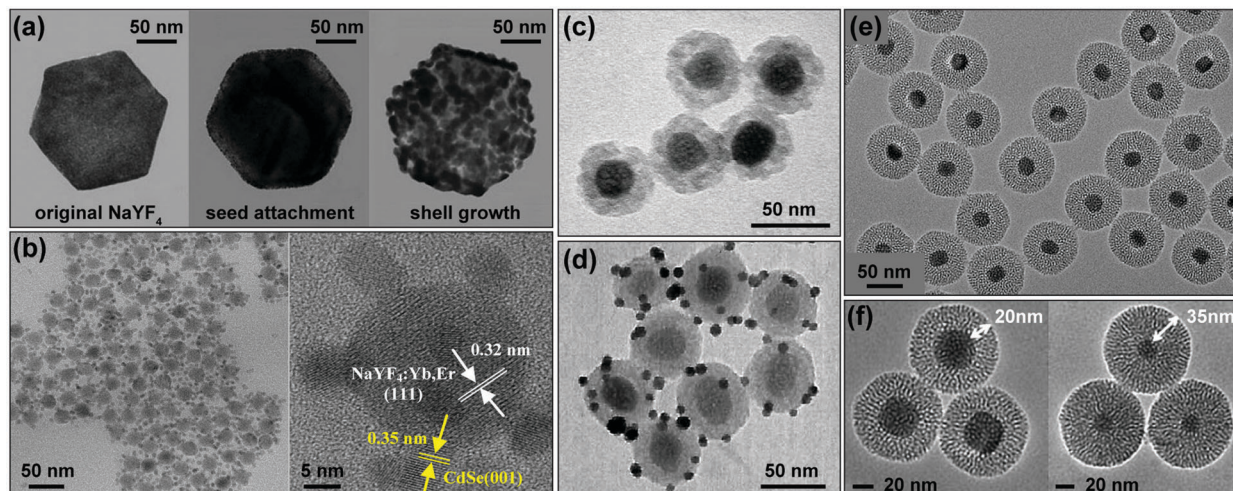


**Fig. 10** TEM images of typical nonepitaxial UC core–shell nanoparticles. (a)  $\text{NaYF}_4\text{:Yb/Tm@Au}$  heterostructure constructed by Huang and Duan *et al.* (b)  $\text{NaYF}_4\text{:Yb/Er@CdSe}$  nanoparticles prepared by Rosei and Perepichka *et al.* (c) Encapsulating quantum dots into the silica shells on  $\text{NaYF}_4\text{:Yb/Er}$  nanoparticles by Li and Zhang *et al.* (d) Coupling gold nanoparticles to  $\text{NaYF}_4\text{:Yb/Er}$  nanoparticles through use of a silica layer by Li and Xiong *et al.* (e) Porous silica coating on  $\text{NaYF}_4\text{:Yb/Er@NaGdF}_4\text{:Yb}$  nanoparticles by Li and Lin *et al.* (f) Tuning the thickness of porous silica shell on  $\text{NaYF}_4\text{:Yb/Tm}$  nanoparticles prepared by Bu and Shi *et al.* Reproduced from ref. 21 and 38–42, respectively.

## 4. Effect of core–shell structure on upconversion

Core–shell nanostructures not only enhance our ability to create efficient UC processes with desirable excitation and emission properties, but also provide a convenient platform for integrating multiple functionalities that offers new opportunities for various applications.

### 4.1 Enhancing emission efficiency

Nanoparticle surfaces featuring structural and compositional discontinuities is typically studded with contaminants and defects that are well-recognized nonradiative energy sinks. By confining lanthanide ions to the interior of an epitaxial core–shell nanoparticle, the UC efficiency can be significantly increased due to largely eliminated energy dissipation to the nanoparticle surface.

The standard strategy for removing threats of surface quenchers is to use a monoshelled nanostructure comprising a lanthanide-doped active core and an undoped protection shell (Fig. 11a). Several groups have observed remarkably enhanced UC emission using an inert shell coating. These reports claimed markedly different enhancement factors ranging from several to hundreds of folds, which is largely owing to the dissimilar core particle size and composition as well as the excitation power density involved in different studies. Another important variable that affects the enhancement factor is the shell thickness. Zhang and Zhao *et al.*<sup>34</sup> carried out a comparative investigation on a series of  $\text{NaYF}_4\text{:Yb/Er@NaGdF}_4$  core–shell nanoparticles with a thin surface coatings in the 0–2.5 nm range. They observed a linear dependence of UC emission intensity on the  $\text{NaGdF}_4$  shell thickness. However, steady enhancement in the UC emission is generally unexpected when using very thick shells. The UC emission intensity often reaches a plateau at a shell

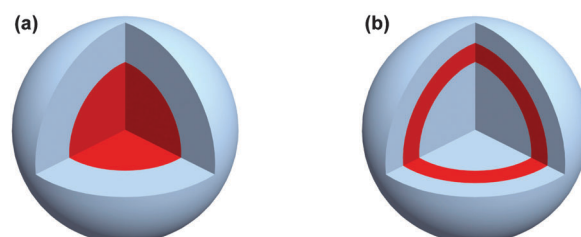


**Fig. 11** Schematic illustration of typical strategies for confining lanthanide ions in core–shell nanoparticles. The red layers comprise the luminescent lanthanide ions. (a) Standard core–shell structure with lanthanide ions confined in the core layer. (b) Sandwich structure with lanthanide ions inserted in the middle layer.

thickness of ~3 nm, corresponding to the critical distance of interaction between surface oscillators and lanthanide dopants.<sup>35</sup>

Multilayered nanoparticles have also been employed to enhance UC efficiencies (Fig. 11b). For example, Zhang and Zhao *et al.*<sup>30</sup> studied  $\text{NaYF}_4\text{@NaYF}_4\text{@NaYF}_4$  core–shell–shell nanoparticles with Yb/Er confined in the inner shell layer, a scheme known as  $\delta$ -doping. They found that  $\delta$ -doping enhances the green-to-red emission intensity ratio of  $\text{Er}^{3+}$  when compared to the  $\text{NaYF}_4\text{:Yb/Er@NaYF}_4$  core–shell counterpart. A decrease in local dopant concentration when the doping position is shifted toward the shell was used to account for the observations. Li *et al.*<sup>44</sup> also investigated the  $\delta$ -doped  $\text{NaYF}_4$  nanoparticles. They attributed an enhancement in the overall UC emission intensity with respect to the standard core–shell structure to a low defect density in the inner shell layer.

In addition to spatially confining dopant ions, nonepitaxial metallic shells have also been harnessed to enhance UC emission, based on the amplification of the excitation flux and on the acceleration of the radiative decay by surface plasmon resonance.<sup>38</sup> However, the reported enhancement factors are

generally limited to several folds, probably due to the side effects of the metal shells that promote the deactivation of the intermediate excited states and quenching of upconverted emission by surface plasmon absorption.<sup>44</sup> Furthermore, the mechanism behind the enhanced luminescence is not well understood. One revealing study is to determine the role of light scattering and plasmonic effect by a judicious design of optical spectroscopy.

Despite previous achievements, the core–shell nanoparticles are still not a match for the corresponding bulk counterparts in term of UC efficiency. A variation in the emission intensity and profile is also frequently observed when the nanoparticles are dispersed in different solvents.<sup>25,45</sup> The poor integrity of the coating layer, such as incomplete or porous shells are mainly responsible for the undesired properties. Another possible reason may be the dopant migration across the core–shell interface towards the surface of the nanoparticle, an assumption that needs to be examined in future studies.

#### 4.2 Increasing functional multiplicity

The core–shell nanostructure provides a straightforward platform for spatially partitioning atoms and molecules. The effect can be harnessed to suppress undesired interference between dissimilar components constituting a core–shell nanoparticle, thereby allowing the rational integration of multiple functionalities into single nanoparticles.

UC nanoparticles with additional luminescence capabilities can be created by integrating epitaxial layers activated by different lanthanide ions. The active-core and active-shell nanostructure was originally proposed to eliminate deleterious cross-relaxation between lanthanide dopants.<sup>33</sup> The effect has been proven useful for combining incompatible optical processes in single nanoparticles without resulting in noticeable luminescence quenching. For example, Chen and Wang *et al.*<sup>46</sup> developed BaF<sub>2</sub>:Yb/Tm@SrF<sub>2</sub>:Nd nanocubes displaying UC and downshifting dual-mode emissions. When compared to the BaF<sub>2</sub>:Yb/Tm/Nd@SrF<sub>2</sub> counterpart featuring homogeneously mixed dopant ions, a more than 10-fold enhancement in emission intensity was reported. In a further development, Zhang and Zhao *et al.*<sup>45</sup> presented a NaGdF<sub>4</sub>:Nd@NaYF<sub>4</sub>@NaGdF<sub>4</sub>:Er/Yb/Nd@NaYF<sub>4</sub> structure. The inert NaYF<sub>4</sub> interlayer was reported to largely suppress interfacial quenching, leading to efficient dual-mode emissions by a single wavelength excitation at 808 nm. The multishell nanoparticles providing dual signalling capabilities would enable more accurate biodetection. In another intriguing demonstration, Branda *et al.*<sup>47</sup> showed that the emission intensity balance between Er<sup>3+</sup> and Tm<sup>3+</sup> in a NaYF<sub>4</sub>:Yb/Er@NaYF<sub>4</sub>:Yb/Tm@NaYF<sub>4</sub> nanoparticle can be adjusted by manipulating the excitation power density. The effect was harnessed to modulate the energy of the upconverted photons for photo-switching of dithienylethene.

In addition to luminescent lanthanide ions, ionic dopants exhibiting various functionalities can be concomitantly included in the core–shell nanostructures. The effect offers the tantalizing possibility to bring together multi-modality imaging capabilities in a miniature nanoparticle system. The combined imaging modalities can function synergistically to allow rapid and

precise investigation of biological activity. For example, with dual-functional probes for magnetic resonance imaging (MRI) and upconversion luminescence (UCL) microscopy, MRIs capable of reconstructing tissues of large volume can be used for a whole body screen to identify regions of interest, thereby reducing the volume of tissues that needs to be scanned by high-resolution UCL imaging.

Gd<sup>3+</sup> and Mn<sup>2+</sup> ions that display outstanding magnetic properties can be straightforwardly incorporated into UC nanoparticles to create dual-functional probes with optical and magnetic imaging capabilities. Bu and Shi *et al.*<sup>48</sup> demonstrated an elegant example by building a NaGdF<sub>4</sub>:Yb/Er@NaGdF<sub>4</sub> core–shell nanoparticle. In their design, the NaGdF<sub>4</sub> shell was used not only to shield the UC processes occurring at the core level, but also to provide maximal exposure of magnetic Gd<sup>3+</sup> ions to surrounding water molecules that lead to an enhanced *T*<sub>1</sub>-weighted MRI contrast. Importantly, the positive image contrast arising from *T*<sub>1</sub> relaxation is not susceptible to interference caused by pathogenic conditions, which generally darken the images to cover the signals generated by negative *T*<sub>2</sub> imaging agents such as iron oxides.

By a careful selection of host lattice and dopant ions, more powerful multimodality probes have been constructed to integrate most of the commonly used imaging capabilities, including positron emission tomography (PET), X-ray computed tomography (CT), and single-photon emission computed tomography (SPECT).<sup>3</sup> A representative example was demonstrated by Li *et al.*<sup>49</sup> who described a core–shell nanoparticle for simultaneous CT, MRI, SPECT, and UCL imaging. The nanoparticle consisted of a NaLuF<sub>4</sub>:Yb/Tm core to offer X-ray attenuation (by Lu) and UCL (by Yb/Tm) properties. A NaGdF<sub>4</sub>:<sup>153</sup>Sm shell was designed to provide magnetism (Gd) and radioactivity (<sup>153</sup>Sm). The four-modality probe has enabled the accurate imaging of tumor angiogenesis in animals at both cell and whole-body levels (Fig. 12).

#### 4.3 Tuning optical properties

A more exciting promise of core–shell nanostructure is for rational optical tuning. By creating a proper conduit, selective energy exchange interactions across the core–shell interface can be achieved, leading to unprecedented control over the excitation and emission spectra of UC nanoparticles (Fig. 13).

Energy transfer through core–shell interface was first demonstrated in UC nanoparticles nonepitaxially covered with organic dyes or QDs, which display intense absorption bands and are able to directly accept energies donated by lanthanide ions, which are typically several nanometers apart (*i.e.* confined in the core levels). In an intriguing example, Gorris and Wolfbeis *et al.*<sup>5</sup> coupled colloidal UC nanoparticle with organic dyes for optical tuning. They showed that the emission peaks of UC nanoparticles can be selectively filtered by surface-capped dye acceptors. By controlling the content of dye molecules in the screen shell layer, the UC emission profile can be precisely manipulated, providing a novel spectral encoding strategy for multiplexed biodetection.

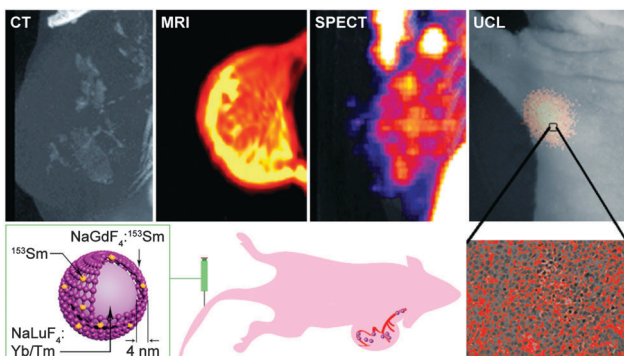


**Fig. 12** Four-modality *in vivo* bioimaging with multifunctional  $\text{NaLuF}_4\text{:Yb/Tm}$ @ $\text{NaGdF}_4\text{:}^{153}\text{Sm}$  core–shell nanoparticles. The nanoparticles were intravenously injected into a mouse. CT and MRI were used to investigate the distribution of the nanoparticles in the tumour blood vessel and in the soft tissue, respectively. The nanoparticles accumulated at the tumour site were further quantified by SPECT. UCL imaging was applied in histochemical analysis of tumour angiogenesis. Reproduced from ref. 49.

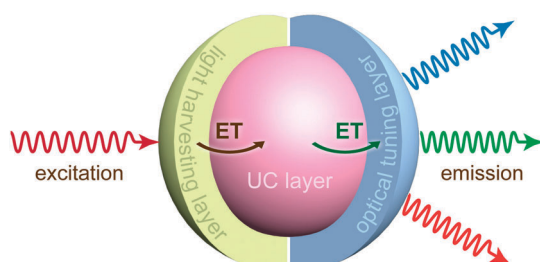


**Fig. 13** General depiction of the core–shell nanoparticle architecture for tuning the UC excitation and emission. Optical components featuring broad and intense absorption in the NIR spectrum can function as antennas to harvest incident light and to transfer their excitation energy to the UC layer. The upconverted energy can also be transferred to other optical entities to generate tunable emissions. ET denotes energy transfer.

Nonradiative Förster interaction is generally believed to mediate the energy transfer from the UC core to the organic chromophores or QDs in the shell layers. However, radiative reabsorption may also significantly contribute to the optical interactions.<sup>5</sup> Notably, radiative reabsorption that is essentially independent of donor–acceptor separation can allow a wide margin of flexibility in core–shell structural design without substantial sacrifice of the energy transfer efficiency.

Surface-covered dye molecules can also transfer energy to lanthanide ions embedded in the crystalline lattice of core nanoparticles. Petoud *et al.*<sup>36</sup> first exploited this effect to enhance the NIR emission of  $\text{Yb}^{3+}$  and  $\text{Nd}^{3+}$  through the use of a  $\text{NaYF}_4\text{:Yb(Nd)}$ @tropolonate core–shell structure. The design combines the antenna effect provided by the chromophoric coating with the advantage of using a crystalline lattice to protect  $\text{Ln}^{3+}$  from nonradiative deactivations, suggesting an innovative strategy for constructing luminescent materials. In a subsequent investigation, Hummelen *et al.*<sup>37</sup> expanded the strategy to develop a dye-sensitized UC nanoparticle system. By optimizing the surface coverage of dye molecules, they

achieved the UC emission of  $\text{NaYF}_4\text{:Yb/Er}$  nanoparticles by NIR excitation across a broad range of wavelengths (740–850 nm). Strikingly, the chromophoric coating boosted the spectral response of the UC nanoparticles in the 720–1000 nm range by 3300 times under low-power excitation.

The use of fluorescent dyes to sensitize UC emission should meet stringent criteria. In addition to being a reasonable match for the excitation band of  $\text{Yb}^{3+}$ , the sensitizer needs to show minimal absorption in the spectral region where UC emission is of interest. As most dye molecules show strong absorption in the UV spectral range, it is unlikely to sensitize NIR-to-UV UC emission by organic dyes. The constraint also precludes the feasibility of sensitizing UC processes by QDs that are characterized by continuous absorption spectra. On a separate note, energy transfer from dye to lanthanide ions typically occurs within a very short distance due to the narrow absorption bands of lanthanide acceptors. To maximize the sensitization process, a compact core–shell configuration (*e.g.* small core particle with a thin surface coating) should be adopted. An elevated lanthanide doping level also promotes energy transfer by increasing the overall absorption strength of lanthanide acceptors.

Reports on energy transfer through epitaxial core–shell interface did not appear until 2009, when Capobianco *et al.*<sup>28</sup> declared an energy transfer from  $\text{Yb}^{3+}$  in a  $\text{NaGdF}_4\text{:Yb}$  shell to  $\text{Er}^{3+}$  in a  $\text{NaGdF}_4\text{:Yb/Er}$  core. However, as the interlayer (core–shell) and intralayer (within the UC core) energy transfers are of the same type ( $\text{Yb} \rightarrow \text{Er}$ ), the effect hardly modifies the UC characteristics other than enhancing the response of the nanoparticles to NIR excitations.

UC fine tuning in epitaxial core–shell nanostructures was first demonstrated by Wang and Liu *et al.*<sup>6</sup> who utilized energy migration through gadolinium sublattice to bridge efficient energy transfer across the core–shell interface (Fig. 14). In this study,  $\text{Yb}/\text{Tm}$  and common lanthanide activators (*e.g.*  $\text{Tb}^{3+}$ ,  $\text{Eu}^{3+}$ ,  $\text{Dy}^{3+}$ , and  $\text{Sm}^{3+}$ ) were doped in the core and shell layers of a  $\text{NaGdF}_4$ @ $\text{NaGdF}_4$  nanostructure, respectively. Upon 980 nm excitation into  $\text{Yb}^{3+}$  ions in the core level, UC emission with tunable wavelengths and lifetimes was observed and attributed to a prescribed  $\text{Yb} \rightarrow \text{Tm} \rightarrow \text{Gd} \rightarrow$  activator energy cascade. Notably, the critical role of Gd sub-lattice in delivering the excitation energy was confirmed by time-resolved luminescence

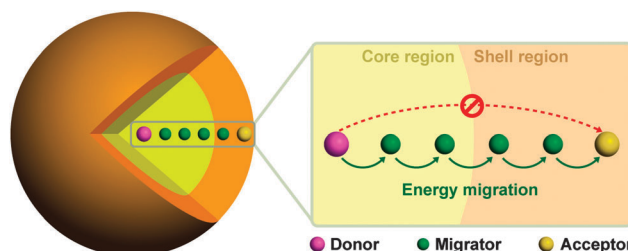


**Fig. 14** Schematic illustration of energy transfer across a core–shell interface by means of energy migration. The network of the energy migrators bridges the donor to acceptor energy transfer by breaking down the long-distance energy transfer into a series of short-distance energy transfers. Reproduced from ref. 6.

spectroscopy in conjunction with control experiments involving the use of Y-diluted Gd sublattice. A minimum Gd content of 30 mol% in the host lattice was identified to initiate the energy migration process.

The combination of energy migration and core–shell structural engineering has been developed as a general strategy for tuning UC properties. For example, Sun and Yan *et al.*<sup>50</sup> synthesized a NaYF<sub>4</sub>:Yb/Er@NaYF<sub>4</sub>:Yb/Nd nanostructure that enables one to sensitize UC emission of Er<sup>3+</sup> by Nd<sup>3+</sup> *via* energy migration through the ytterbium sublattice. The inclusion of Nd<sup>3+</sup> sensitizer that displays several absorption peaks spanning from deep red to NIR can shift the excitation to a shorter wavelength. The effect is useful for eliminating the overheating effect in the context of bioapplications typically associated with a 980 nm laser to achieve excitation of Yb-sensitized UC nanoparticles. In parallel mechanistic investigations, Liu *et al.*<sup>51</sup> and Wang *et al.*<sup>52</sup> confirmed the role of the Yb sublattice in mediating the energy transfer from Nd<sup>3+</sup> to Er<sup>3+</sup>. It is worth noting that the minimum content of Yb needed to initiate this energy exchange process is much lower (<10 mol%) when compared to the Gd system. The phenomenon is largely due to the stronger optical transition in Yb<sup>3+</sup> ions, which results in a longer critical distance of interaction between Yb<sup>3+</sup> pairs.

A prominent advantage of using epitaxial core–shell nanostructure to tune UC is that all the optical components can be appreciably protected from nonradiative deactivations. For example, Wang and Liu *et al.*<sup>35</sup> showed that a NaYF<sub>4</sub> protection layer can be readily coated around NaGdF<sub>4</sub>:Yb/Tm@NaGdF<sub>4</sub>:A (A = Tb<sup>3+</sup>, Eu<sup>3+</sup>, Dy<sup>3+</sup>, and Sm<sup>3+</sup>) core–shell nanoparticles to eliminate the dissipation of excitation energy at the nanoparticle surface. The effect renders energy trapping by the activator ions a dominant destination of the migrating energy, leading to enhanced optical emissions. In another interesting study, Yao *et al.*<sup>53</sup> built a NaYF<sub>4</sub>:Yb/Er@NaYF<sub>4</sub>:Yb@NaNdF<sub>4</sub>:Yb core–shell–shell nanoparticle to enhance the Nd-sensitized UC. They showed that the insertion of a buffer layer (NaYF<sub>4</sub>:Yb) between the sensitization layer (NaNdF<sub>4</sub>:Yb) and the emission layer (NaYF<sub>4</sub>:Yb/Er) can largely suppress the cross-relaxation between activator (Er<sup>3+</sup>) and sensitizer (Nd<sup>3+</sup>) at the core–shell interface. Importantly, the desired energy transfer across the core–shell interface was only marginally affected due to the Yb sub-lattice in the buffer layer.

Epitaxial core–shell nanostructure also permits multiple optical components to come together to create unprecedented UC processes. Our group substantiated this effect by developing a NaYbF<sub>4</sub>@Na(Yb, Gd)F<sub>4</sub>@NaGdF<sub>4</sub> core–shell–shell structure for the simultaneous tuning of UC excitation and emission.<sup>52</sup> In this design, the core, inner shell, and outermost shell layers were doped with Nd<sup>3+</sup>, Tm<sup>3+</sup> (or Er<sup>3+</sup>, Ho<sup>3+</sup>), and Tb<sup>3+</sup> (or Eu<sup>3+</sup>, Dy<sup>3+</sup>) to realize light harvesting, upconverting, and optical tuning processes, respectively. With the assistance of the Yb and Gd sublattices in the host matrix, these optical processes collaboratively give rise to the tunable UC emissions spanning from UV to deep red by biocompatible 808 nm excitation. Intriguingly, a colour kinetic UC nanoparticle was also demonstrated by employing a multishelled structure (Fig. 15) with the capability of encoding dual upconverting ions (Ho<sup>3+</sup> and Tm<sup>3+</sup>). To manipulate the Nd-sensitized UC process, the Ho<sup>3+</sup> and Nd<sup>3+</sup> ions were connected by an array of Yb<sup>3+</sup> ions,

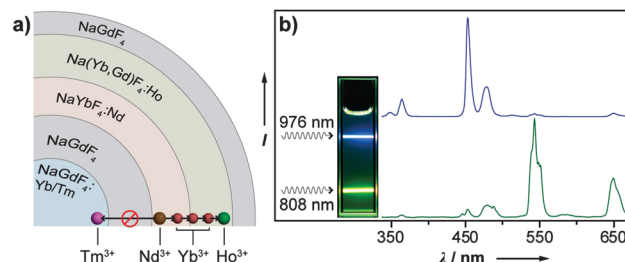


Fig. 15 (a) Schematic design of colour kinetic UC nanoparticles through the use of multishelled structure. (b) Emission spectra of the nanoparticles under excitation at 808 and 976 nm, respectively. Inset: photograph of the corresponding nanoparticle colloids. Reproduced from ref. 52.

whereas the Tm<sup>3+</sup> and Nd<sup>3+</sup> ions were separated by a NaGdF<sub>4</sub> interlayer. The nanoparticles are able to emit light of distinct colours in response to excitation at 808 and 976 nm, respectively.

## 5. Conclusions

The ability to create UC emission by doping lanthanide ions into bulk materials has been long recognized. The extent to which the scope of UC can be expanded, however, has been appreciated only in recent years when nanofabrication became increasingly routine. In comparison with conventional bulk counterparts, UC core–shell nanoparticles can be constructed using a rather wide range of optical components, including most lanthanide ions as well as organic dyes and QDs, leading to highly designable and tunable UC properties. The effect has enabled better understanding and manipulation of complicated energy transfer processes in solid matters, in parallel with providing new opportunities for advanced biological applications. One important work in the future is to develop advanced approaches for probing the structure of core–shell nanoparticles with high resolution and accuracy, which should contribute to an integral picture of the delicate structure–property relationships. Rational integration of diverse optical components into a single nanoparticle without creating noticeable interfacial defects represents another key step toward fully realizing the potential of core–shell nanostructural engineering for UC applications.

## Acknowledgements

F.W. acknowledges City University of Hong Kong (No. 7200317, 9610257, and 9667073), the Research Grants Council of Hong Kong (CityU 109413), National Natural Science Foundation of China (No. 21303149 and 51332008), and the Science Technology and Innovation Committee of Shenzhen Municipality (JCYJ20130401145617278) for supporting this work.

## Notes and references

- 1 M. Haase and H. Schäfer, *Angew. Chem., Int. Ed.*, 2011, **50**, 5808.
- 2 X. Huang, S. Han, W. Huang and X. Liu, *Chem. Soc. Rev.*, 2013, **42**, 173.

- 3 G. Chen, H. Qiu, P. N. Prasad and X. Chen, *Chem. Rev.*, 2014, **114**, 5161.
- 4 K. Kompe, H. Borchert, J. Storz, A. Lobo, S. Adam, T. Moller and M. Haase, *Angew. Chem., Int. Ed.*, 2003, **42**, 5513.
- 5 H. H. Gorris, R. Ali, S. M. Saleh and O. S. Wolfbeis, *Adv. Mater.*, 2011, **23**, 1652.
- 6 F. Wang, R. Deng, J. Wang, Q. Wang, Y. Han, H. Zhu, X. Chen and X. Liu, *Nat. Mater.*, 2011, **10**, 968.
- 7 G. Blasse and B. C. Grabmaier, *Luminescent Materials*, Springer, Berlin, 1994.
- 8 R. T. Wegh, H. Donker, K. D. Oskam and A. Meijerink, *Science*, 1999, **283**, 663.
- 9 F. Auzel, *Chem. Rev.*, 2004, **104**, 139.
- 10 Q. Liu, B. Yin, T. yang, Y. Yang, Z. Shen, P. Yao and F. Li, *J. Am. Chem. Soc.*, 2013, **135**, 5029.
- 11 A. Shalav, B. S. Richards and M. A. Green, *Sol. Energy Mater. Sol. Cells*, 2007, **91**, 829.
- 12 J. Wang, R. Deng, M. A. MacDonald, B. Chen, J. Yuan, F. Wang, D. Chi, T. S. Hor, P. Zhang, G. Liu, Y. Han and X. Liu, *Nat. Mater.*, 2014, **13**, 157.
- 13 Y.-W. Zhang, X. Sun, R. Si, L.-P. You and C.-H. Yan, *J. Am. Chem. Soc.*, 2005, **127**, 3260.
- 14 H.-X. Mai, Y.-W. Zhang, R. Si, Z.-G. Yan, L.-d. Sun, L.-P. You and C.-H. Yan, *J. Am. Chem. Soc.*, 2006, **128**, 6426.
- 15 G. Chen, J. Shen, T. Y. Ohulchansk, N. J. Patel, A. Kutikov, Z. Li, J. Song, R. K. Pandey, H. Ågren, P. N. Prasad and G. Han, *ACS Nano*, 2012, **6**, 8280.
- 16 Y. I. Park, J. H. Kim, K. T. Lee, K.-S. Jeon, H. B. Na, J. H. Yu, H. M. Kim, N. Lee, S. H. Choi, S.-I. Baik, H. Kim, S. P. Park, B.-J. Park, Y. W. Kim, S. H. Lee, S.-Y. Yoon, I. C. Song, W. K. Moon, Y. D. Suh and T. Hyeon, *Adv. Mater.*, 2009, **21**, 4467.
- 17 X. Ye, J. E. Collins, Y. Kang, J. Chen, D. T. N. Chen, A. G. Yodh and C. B. Murray, *Proc. Natl. Acad. Sci. U. S. A.*, 2010, **107**, 22431.
- 18 X. Wang, J. Zhuang, Q. Peng and Y. Li, *Nature*, 2005, **437**, 121.
- 19 F. Zhang, Y. Wan, T. Yu, F. Zhang, Y. Shi, S. Xie, Y. Li, L. Xu, B. Tu and D. Zhao, *Angew. Chem., Int. Ed.*, 2007, **46**, 7976.
- 20 H.-X. Mai, Y.-W. Zhang, L.-D. Sun and C.-H. Yan, *Chem. Mater.*, 2007, **19**, 4514.
- 21 Z. Li, Y. Zhang and S. Jiang, *Adv. Mater.*, 2008, **20**, 4765.
- 22 N. J. J. Johnson, W. Oakden, G. J. Stanisz, R. Scott Prosser and F. C. J. M. van Veggel, *Chem. Mater.*, 2011, **23**, 3714.
- 23 W. Zheng, S. Zhou, Z. Chen, P. Hu, Y. Liu, D. Tu, H. Zhu, R. Li, M. Huang and X. Chen, *Angew. Chem., Int. Ed.*, 2013, **52**, 6671.
- 24 F. Wang, Y. Han, C. S. Lim, Y. H. Lu, J. Wang, J. Xu, H. Chen, C. Zhang, M. Hong and X. Liu, *Nature*, 2010, **463**, 1061.
- 25 F. Wang, J. Wang and X. Liu, *Angew. Chem., Int. Ed.*, 2010, **49**, 7456.
- 26 F. Wang, R. Deng and X. Liu, *Nat. Protoc.*, 2014, **9**, 1634.
- 27 G.-S. Yi and G.-M. Chow, *Chem. Mater.*, 2007, **19**, 341.
- 28 F. Vetrone, R. Naccache, V. Mahalingam, C. G. Morgan and J. A. Capobianco, *Adv. Funct. Mater.*, 2009, **19**, 2924.
- 29 P. Huang, W. Zheng, S. Zhou, D. Tu, Z. Chen, H. Zhu, R. Li, E. Ma, M. Huang and X. Chen, *Angew. Chem., Int. Ed.*, 2014, **53**, 1252.
- 30 X. Li, D. Shen, J. Yang, C. Yao, R. Che, F. Zhang and D. Zhao, *Chem. Mater.*, 2013, **25**, 106.
- 31 N. J. Johnson, A. Korinek, C. Dong and F. C. J. M. van Veggel, *J. Am. Chem. Soc.*, 2012, **134**, 11068.
- 32 H.-X. Mai, Y.-W. Zhang, L.-D. Sun and C.-H. Yan, *J. Phys. Chem. C*, 2007, **111**, 13721.
- 33 H.-S. Qian and Y. Zhang, *Langmuir*, 2008, **24**, 12123.
- 34 F. Zhang, R. Che, X. Li, C. Yao, J. Yang, D. Shen, P. Hu, W. Li and D. Zhao, *Nano Lett.*, 2012, **12**, 2852.
- 35 Q. Su, S. Han, X. Xie, H. Zhu, H. Chen, C. K. Chen, R. S. Liu, X. Chen, F. Wang and X. Liu, *J. Am. Chem. Soc.*, 2012, **134**, 20849.
- 36 J. Zhang, C. M. Shade, D. A. Chengelis and S. Petoud, *J. Am. Chem. Soc.*, 2007, **129**, 14834.
- 37 W. Zou, C. Visser, J. A. Maduro, M. S. Pshenichnikov and J. C. Hummelen, *Nat. Photonics*, 2012, **6**, 560.
- 38 H. Zhang, Y. Li, I. A. Ivanov, Y. Qu, Y. Huang and X. Duan, *Angew. Chem., Int. Ed.*, 2010, **49**, 2865.
- 39 C. Yan, A. Dadvand, F. Rosei and D. F. Perepichka, *J. Am. Chem. Soc.*, 2010, **132**, 8868.
- 40 Z. Li, L. Wang, Z. Wang, X. Liu and Y. Xiong, *J. Phys. Chem. C*, 2011, **115**, 3291.
- 41 C. Li, D. Yang, P. Ma, Y. Chen, Y. Wu, Z. Hou, Y. Dai, J. Zhao, C. Sui and J. Lin, *Small*, 2013, **9**, 4150.
- 42 J. Liu, W. Bu, S. Zhang, F. Chen, H. Xing, L. Pan, L. Zhou, W. Peng and J. Shi, *Chem. – Eur. J.*, 2012, **18**, 2335.
- 43 N. J. Johnson, N. M. Sangeetha, J. C. Boyer and F. C. van Veggel, *Nanoscale*, 2010, **2**, 771.
- 44 Z. Li, W. Park, G. Zorzetto, J. S. Lemaire and C. J. Summers, *Chem. Mater.*, 2014, **26**, 1770.
- 45 X. Li, R. Wang, F. Zhang, L. Zhou, D. Shen, C. Yao and D. Zhao, *Sci. Rep.*, 2013, **3**, 3536.
- 46 D. Chen, Y. Yu, F. Huang, H. Lin, P. Huang, A. Yang, Z. Wang and Y. Wang, *J. Mater. Chem.*, 2012, **22**, 2632.
- 47 J.-C. Boyer, C.-J. Carling, B. D. Gates and N. R. Branda, *J. Am. Chem. Soc.*, 2010, **132**, 15766.
- 48 F. Chen, W. Bu, S. Zhang, J. Liu, W. Fan, L. Zhou, W. Peng and J. Shi, *Adv. Funct. Mater.*, 2013, **23**, 298.
- 49 Y. Sun, X. Zhu, J. Peng and F. Li, *ACS Nano*, 2013, **7**, 11290.
- 50 Y.-F. Wang, G.-Y. Liu, L.-D. Sun, J.-W. Xiao, J.-C. Zhou and C.-H. Yan, *ACS Nano*, 2013, **7**, 7200.
- 51 X. Xie, N. Gao, R. Deng, Q. Sun, Q. H. Xu and X. Liu, *J. Am. Chem. Soc.*, 2013, **135**, 12608.
- 52 H. Wen, H. Zhu, X. Chen, T. F. Hung, B. Wang, G. Zhu, S. F. Yu and F. Wang, *Angew. Chem., Int. Ed.*, 2013, **52**, 13419.
- 53 Y. Zhong, G. Tian, Z. Gu, Y. Yang, L. Gu, Y. Zhao, Y. Ma and J. Yao, *Adv. Mater.*, 2014, **26**, 2831.